ELSEVIER

Journal of Physics and Chemistry of Solids 64 (2003) 1317–1331

JOURNAL OF PHYSICS AND CHEMISTRY OF SOLIDS

www.elsevier.com/locate/jpcs

On the mechanism of the interaction between oxygen and close-packed single-crystal aluminum surfaces

Yu.F. Zhukovskii[a,b,1,*], P.W.M. Jacobs[b], M. Causá[c]

[a]*Institute of Solid State Physics, University of Latvia, 8 Kengaraga, LV-1063 Riga, Latvia*
[b]*Department of Chemistry, The University of Western Ontario, London, Ont., Canada N6A 5B7*
[c]*Department of Sciences and Advanced Technologies, University 'Amedeo Avogadro', I-15100 Alessándria, Italy*

Received 19 April 2002; accepted 6 April 2003

Abstract

Using periodic first principles simulations we investigate the interaction of oxygen molecules with both regular Al(111) and Al(001) surfaces as well as a stepped Al(111) substrate. The limitation of this approach is the use of thin metallic slabs with a limited range for their coverage by adsorbed oxygen. The advantage is the detailed modeling that is possible at an atomic level. On the regular Al(111) surface, we have been able to follow the oxidation process from the approach of O_2 molecules to the surface, through the chemisorption and absorption of O atoms, up to the formation of first Al_2O_3 formula units. An energetically feasible mechanism for the formation of these Al_2O_3 'molecules' is proposed but their aggregation to Al_2O_3 growth nuclei can only be surmised. On the Al(001) surface, absorption of oxygen atoms occurs more readily without any restrictions on the density of their surface overlayer, in agreement with the failure to observe a distinct chemisorption stage for O on Al(001) experimentally. The stepped Al(111) surface contains both {111} and {001} microfacets: the latter are obviously preferred for penetration of the oxygen adatoms into the subsurface space of the substrate. Before considering the O/Al interfaces the computational method is tested thoroughly by simulations on bulk Al and close-packed aluminum surfaces.
© 2003 Elsevier Science Ltd. All rights reserved.

1. Introduction

Because of the high affinity of Al towards O the exposure of a clean aluminum surface to gaseous oxygen results in the rapid formation of a coherent, pore-free film of Al_2O_3 [1]. Extremely slow diffusion of oxygen through the growing oxide film limits its thickness to only 0.1 μm, but being chemically inert and mechanically durable this film is responsible for the widespread use of aluminum in technological and domestic applications.

Initially, theoretical studies of the oxidation of aluminum were limited to kinetic and thermodynamic considerations. Phenomenological models [2–4] gradually became supplemented by electronic structure calculations of the O/Al interface, based on both the Hartree-Fock (HF) method [5–10] and Density Functional Theory (DFT) [11–24]. HF calculations were mainly performed on various kinds of finite cluster models, while with DFT methods periodic slab models were preferred. In addition to electronic structure simulations, effective-medium model potentials obtained from DFT calculations were used to describe the mobility of oxygen adatoms on the Al(111) surface using molecular dynamics (MD) [25,26]. A lattice-dynamical model based on pair interactions was used by both Strong et al. [27] to interpret the results of high-resolution energy-loss spectroscopy (HREELS) and Chakarova et al. [28] to perform Monte-Carlo simulations of the initial oxidation of Al(111). Results from surface-extended X-ray absorption fine structure (SEXAFS) by Stöhr et al. [29] were analyzed

* Corresponding author. Tel.: +371-718-7480; fax: +371-718-2778.
E-mail address: quantzh@latnet.lv (Yu.F. Zhukovskii).
[1] Web: http://www.cfi.lu.lv/teor/zhuk.html

0022-3697/03/$ - see front matter © 2003 Elsevier Science Ltd. All rights reserved.
doi:10.1016/S0022-3697(03)00156-2

using a microscopic model, in order to clarify structural transformations during Al(111) oxidation. MD simulations have been also performed to interpret angle-resolved secondary ion mass spectrometry measurements (ARSIMS) of oxygen interaction with Al(001) surface [30].

Modern experimental studies using scanning tunneling microscopy (STM) [31,32], normal-incidence standing X-ray wave-field absorption (NISXW) [33], X-ray photoelectron spectroscopy (XPS) [9,34,35], low energy electron diffraction (LEED) [36,37], metastable impact electron spectroscopy (MIES) [38], primary zero loss electron emission spectroscopy (PZL) [39], and HREELS experiments [27,40,41] have helped to clarify important details of the initial stages of aluminum oxidation. Our theoretical simulations are related to these investigations whenever possible.

This paper concentrates on the most important results of our DFT study on the interaction between close-packed aluminum surfaces and oxygen, up to the formation of separated Al_2O_3 formula units on a regular Al(111) substrate. The regular O/Al(111) interface is considered as a model system to study the beginning of aluminum oxidation because of a structural peculiarity: when an oxygen atom crosses the interface plane, the Al/O bond has a length (1.65 Å), which is less than the sum of the atomic radii of O (0.6 Å) and Al (1.25 Å) [1]. Thus, some reconstruction of substrate is necessary to permit inward penetration of O_{ads} atoms and this takes a certain time, which may be sufficient to allow experimental measurements to be made on the oxygen adsorbate. Moreover, the Al_2O_3 formula unit and a regular Al(111) substrate are compatible spatially, since their point symmetry groups are D_{3h} and C_{3v}, respectively. Therefore comparatively simple periodic models may be used for the simulation of the initial stage of aluminum oxide nucleation. For further details about the simulations on regular O/Al(111) interface the reader is referred to our recent paper [21]. We also refer to the most important results on this system that have been published recently [22–24,28].

Interpretation of experimental data for the O/Al(001) interface is much more difficult. For example, it is not possible to distinguish by any experimental method the elementary stages of chemisorption, absorption and oxide nucleation [1]. The most probable reason is that, unlike the O/Al(111) interface, no structural reconstruction of the Al(001) surface is necessary for the penetration of O_{ads} atoms into the substrate: for an adatom, lying in the middle of the square unit cell (UC) of the Al(001) plane, the Al/O bond has a length of 2.025 Å which is larger than the sum of the atomic radii of O and Al atoms (1.85 Å). In addition, no simple periodic model may be constructed for the [(Al_2O_3),O]/Al(001) system due to the different symmetry of the Al_2O_3 formula units and the substrate (which are D_{3h} and C_{4h}, respectively). Consequently, we did not consider the stage of initial oxide nucleation on this close-packed substrate at all.

As to the stepped O/Al(111) interface, this contains both {111} and {001} microfacets which also occur in islands homoepitaxially grown on the Al(111) surface [42,43]. We consider here the interaction between oxygen and stepped substrate, beginning with atomic chemisorption, only up to the stage of absorption and internal diffusion of O atoms, since computational restrictions on calculations on such a complicated system, do not allow us to simulate either the dissociation of O_2 molecules over the stepped substrate or initial oxide nucleation on this surface.

2. Computational details

In the CRYSTAL98 code [44] the periodic wave functions are defined as CO LCGTF (crystalline orbitals formed from linear combinations of Gaussian-type functions). To perform DFT calculations on bulk aluminum and slab models of close-packed Al surfaces, we used the following functionals in the Kohn–Sham equations: (i) LDA/VWN local spin-density exchange (Dirac [45]) with a correlation formula suggested by Vosko et al. [46] and (ii) B/PWGGA non-local exchange (Becke [47]) with a correlation potential constructed by Perdew and Wang [48] according to the Generalized Gradient Approximation. However, to perform calculations on heterogeneous O/Al interfaces we have chosen GGA potentials only, which depend not only on the electron density but also on its gradients. Recently this approximation was shown to give reasonable results in periodic CRYSTAL calculations on metal reactivity towards gases [49,50]. The stability of the Fermi level ε_F during the self-consistent-field (SCF) procedure is much improved in the CRYSTAL98 code by replacing the Heaviside 0 K occupation function $\Theta\{\varepsilon_F - \varepsilon(\mathbf{k})\}$ by a linear approximation to the finite temperature Fermi–Dirac occupation function $f_T\{\varepsilon_F - \varepsilon(\mathbf{k})\}$. This substitution, when combined with level shifting [51], effectively removes the inherent instability associated with SCF calculations on metals and small band-gap semiconductors. We also took advantage of the convergence stabilizer, which mixes current and previous Kohn–Sham matrices at each SCF cycle [52]. One of the crucial points in calculations on metals is a correct choice of reciprocal-space integration parameters: optimum values of shrinking factors for Al were found to be 16 for both the Monkhorst and Pack [53] and Gilat [54] nets.

All-electron basis sets (BSs) consisting of GTFs were used for both aluminum and oxygen. That for Al (8-8-311G) was based on a BS used previously [55], but modified by adding a 3d-type polarization function and then re-optimizing valence and virtual shells to achieve a minimum total energy. To take into account quantum size effects the outer valence 3sp and virtual 4sp and 3d shells in the external layers of Al slabs, were made slightly more diffuse (as suggested by Boettger et al. [56]) and then these GTFs

were again re-optimized. This resulted in a more homogeneous electron distribution and improved SCF convergence. The BS for oxygen (8-511G) was obtained by re-optimizing that used earlier in CRYSTAL investigations of MgO polymorphs [57] but modified by adding a 3d polarization function. To optimize the basis sets and the geometry of the various slab configurations we used a procedure introduced by Heifets et al. [58] that interfaces with CRYSTAL calculations a conjugate gradient optimization technique [59] using numerical computation of derivatives.

3. Results for pure aluminum

3.1. Bulk crystal

Aluminum has a face-centered cubic (*fcc*) structure with lattice constant 4.05 Å and a nearest-neighbor distance between Al atoms of 2.86 Å. Table 1 compares our calculations on bulk Al [60], using both the LDA/VWN and B/PWGGA exchange-correlation functionals, with experimental data and previously published theoretical results. This table confirms conclusions drawn earlier from calculations on bulk Cu [50], Mg [61] and Pt [62] and that the LDA tends to slightly overestimate binding energies and underestimate bond distances. Our B/PWGGA calculated values of the lattice constant a_o, bulk modulus B and cohesive energy E_{coh} are in a good quantitative agreement with experiment. Individual elastic constants and particularly the shear constants are more sensitive to the BS (because of the distortion of the unit cell involved in their calculation) and are consequently much harder to calculate accurately. c_{44} is also sensitive to the sampling of Brillouin zone: using current computing resources we were limited to the shrinking factors of 16. On the whole, our re-optimized Al BS does as well or better than previous CRYSTAL calculations on Al bulk properties [55].

Table 1
Properties of aluminum crystal (lattice constant a_o, bulk modulus B, elastic constants c_{11}, c_{12}, c_{44}, and cohesive energy E_{coh}) calculated for different DFT exchange-correlation functionals and their comparison with experimental and other theoretical data

Method used	a_o, (Å)	B (GPa)[a]	c_{11} (GPa)	c_{12} (GPa)	c_{44} (GPa)	E_{coh} (eV)
LDA/VWN	4.00	78.7	94.0	67.0	11.6	3.93
B/PWGGA	4.05	76.7	104	69.6	16.5	3.50
Experiment[b]	4.05[c]	76.2[d]	108[d]	62.0[d]	28.3[d]	3.34[d]
Theoretical	4.00[e]	77.8[e]	81.7[f]	72.1[f]	16.0[f]	3.60[e]

[a] 1 GPa = 2.29371×10^{-4} Hartree/Å^3 = 1 GJ/m^3 = 10^{10} dyne/cm^2 = 10^{-2} Mbar.
[b] Experimental values were obtained in the temperature interval 273–298 K.
[c] Straumanis and Woodard [68].
[d] Tallon and Wolfenden [69].
[e] Towler et al. [55].
[f] Sutton and Chen [70].

Fig. 1 shows the calculated band structure (BSTR) of bulk Al along principal directions in the first Brillouin zone (BZ) of the body-centered cubic (*bcc*) reciprocal lattice. Since the two different exchange and correlation functionals used produce very similar electron densities and band structures (cf. [55]) we have shown the calculated BSTR from the B/PWGGA functional only. Fig. 1 is clearly in good agreement with the band structures of bulk Al published earlier by Singhal and Callaway [63] and by Szmulowicz and Segall [64]. A quantitative comparison of our results with BSTR parameters published previously is given in Table 2 and these verify that our CRYSTAL simulation gives as good an account of the electronic structure of aluminum as do other calculations.

3.2. Slab models

In our previous paper [60] we have described in detail slab models of all three kinds of pure aluminum substrate mentioned above: the regular and stepped Al(111) as well as regular Al(001) surfaces. The Al(111) slab is characterized by the layer stacking *ABCA*… and non-relaxed interlayer spacing between (111) planes $a_o/\sqrt{3} \approx 2.34$ Å (only three layers are shown in Fig. 2). The less densely-packed Al(001) slab is described by the layer stacking *ABA*… and non-relaxed interlayer spacing $a_o/2 \approx 2.025$ Å (Fig. 3 with the same three layers). To construct the stepped Al(111) slab (Fig. 4) we have cut every second row from the outer layers of a regular Al(111) slab, which are parallel to the (110) crystallographic axis (cf. Figs. 2(a) and 4(a)). The slab model with regular steps containing both {111} and {001} microfacets may be described by the point symmetry group D_{2d}.

Since low-index surfaces of single-crystal aluminum do not exhibit spontaneous reconstruction in a chemically inert environment [65] we investigated only vertical relaxation of the outer layers of Al slabs containing 3, 5 and 7 layers. Table 3 gives these relaxations, as well as surface energies, the charges on surface atoms and Mulliken bond populations. The distributions of electrostatic potential (EP) across the regular and stepped (111) as well as regular (001) slabs which were described by us recently [60] show that only the surface-layer EP is significantly perturbed by the surface. While convergence with respect to the number of layers cannot be claimed, the calculated surface energy of 7-layer slabs is in a good agreement with experiment [66]. The other properties in Table 3 are in satisfactory agreement with experiment and/or results of earlier calculations, bearing in mind the rather large uncertainties associated with the determination of surface properties other than the surface energy. We conclude that, at least as far as configuration energies are concerned, our model should

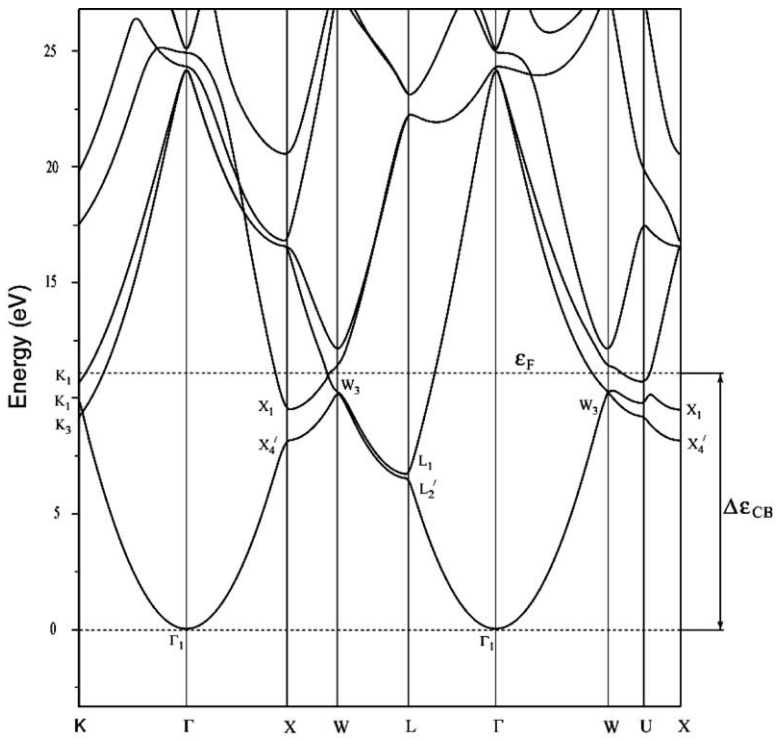

Fig. 1. Band structure of bulk aluminum near the Fermi level calculated along a line joining points of high symmetry in the first Brillouin zone, in the same order as used earlier by Singhal and Callaway [62].

give an adequate description of the adsorption of oxygen and its subsequent reaction with the regular and stepped Al(111) and regular Al(001) surfaces.

4. Adsorption and reaction of oxygen on the regular Al(111) substrate

To simulate the adsorption of molecular oxygen we used mainly a 2×1 supercell (SC), with one O_2 molecule per SC (Fig. 2). This model corresponds to a monolayer of chemisorbed oxygen atoms after dissociation of O_2 molecules. Some calculations with a 2×2 SC and atomic coverage $\theta_O = 0.25$ were performed in order to study the penetration of oxygen adatoms into the substrate at lower coverages.

The simulation of oxygen adsorption began with a free O_2 molecule with optimized bond-length 1.23 Å just above the surface (see (a) and (b) configurations in Table 4). The most favorable configuration for an adsorbed O_2 molecule with fixed intramolecular distance was found to be a vertical rather than a horizontal one, in agreement with the results of an earlier LEED study [37]. We found the *fcc* site above

Table 2
Calculated values of the Fermi level ε_F and of the band energies at some high-symmetry points in the first Brillouin zone of bulk aluminum (Fig. 1) compared with earlier results of calculations and experimental data from angle-resolved photoemission experiments. Because of the choice of energy zero, ε_F is the width of the conduction band ($\Delta\varepsilon_{CB}$)

Source of data (method)	Energy (in eV) referred to bottom of conduction band				
	ε_F	K	X	W	L
This paper (LCGTF)	11.0	$K_1$10.8, $K_1$9.6, $K_3$9.0	$X_1$9.5, X_4'8.2	$W_3$9.8	$L_1$6.8, L_2'6.2
Singhal and Callaway [63] (LCGTF)	11.1	$K_1$10.9, $K_1$9.8, $K_3$9.0	$X_1$9.5, X_4'8.0	$W_3$10.1	$L_1$6.7, L_2'6.5
Szmulowicz and Segall [64] (APW)	11.1	$K_1$10.5, $K_1$9.7, $K_3$9.0	$X_1$9.5, X_4'8.3	$W_3$9.7	$L_1$6.7, L_2'6.5
Levinson et al. [71] (ARUPS experiments)	10.6 ± 0.2	$K_1$10.4	$X_1$9.5, X_4'7.3	$W_3$9.7	L_2'6.1

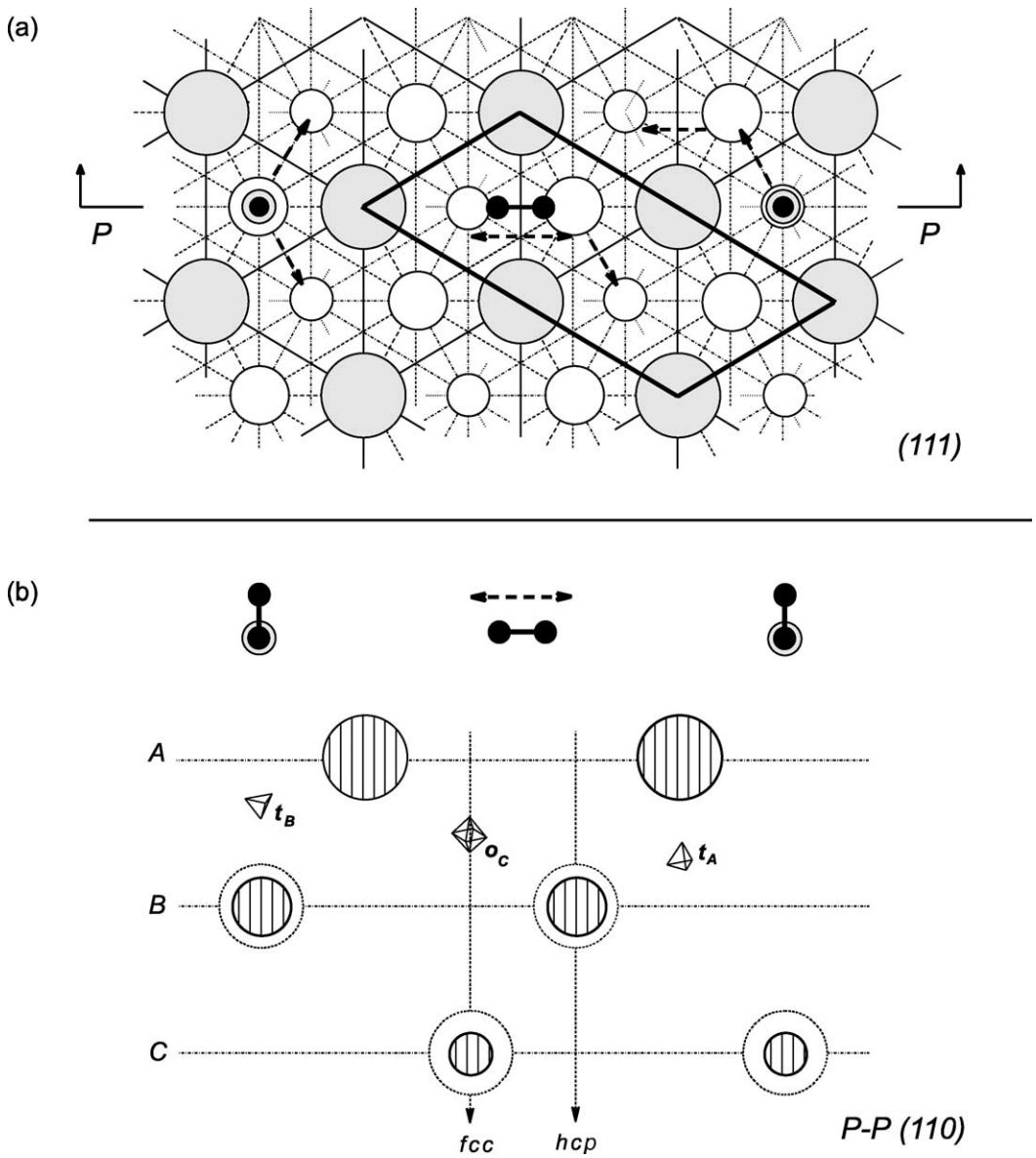

Fig. 2. Periodic model for the adsorption of an O_2 molecule (shown in black) on the perfect Al(111) slab with three possible adsorption sites: one a horizontal position over the 'bridge' between nearest Al atoms on the surface and the other two vertical positions above *fcc* and *hcp* sites (as shown in (b)). The most probable trajectories for dissociation are shown in (a) by dashed arrows. (a) Top view of the Al(111) substrate. Largest gray circles denote Al atoms in the top layer (A) and smaller white circles Al atoms in the next subsurface layers B and C. All nearest-neighbor atoms are joined by straight lines (used for surface atoms only) or by dashed lines. The 2×1 surface supercell is marked by thicker lines. (b) Cross-section of the same model as shown in (a) along the P–P(110) plane including all three molecular configurations. Dash–dot arrows indicate probable trajectories for absorption of oxygen ions. The small tetrahedra and octahedra show interstitial sites t_A, t_B and o_C of tetrahedral and octahedral symmetry, which are the preferred sites for the location of metastable absorbed O^-_{ads} ions.

the octahedral center o_C shown in Fig. 2(b) to be slightly favored (by 0.05 eV) over the hexagonal close-packed (*hcp*) site above the tetrahedral center t_B. Calculations were performed on both singlet and triplet states, the latter being more stable by 0.9–1.05 eV, which may be compared to an energy difference of 1.14 eV in free O_2 molecules. Adsorption of molecular oxygen is accompanied by the transfer of about 1 e per molecule from external aluminum atoms, resulting in the formation of $(O_2^-)_{ads}$ ions. Honkala and Laasonen [20] also predict their formation in the O_2/Al(111) interface. A comprehensive DFT study of the multidimensional adiabatic potential-energy hypersurface

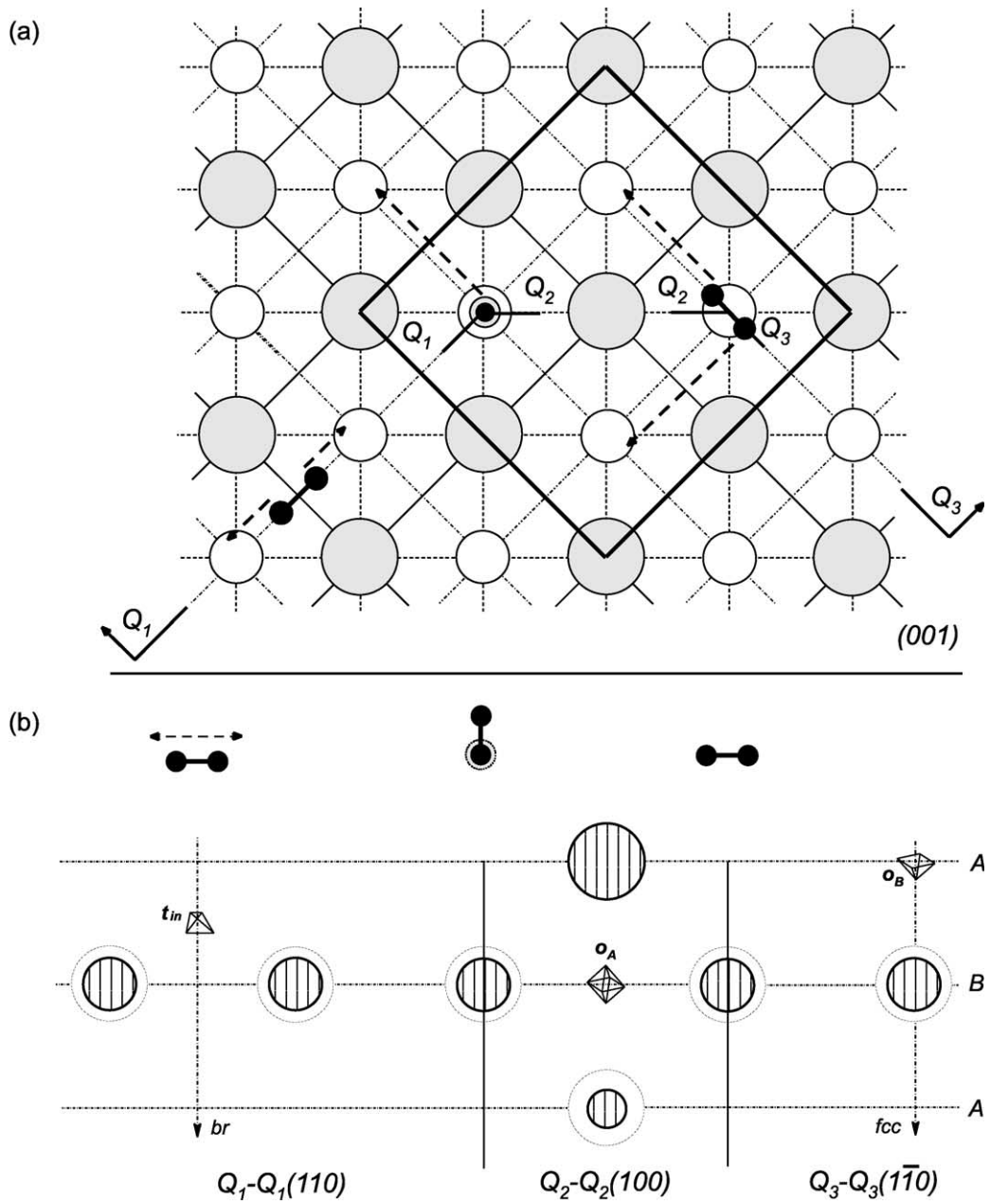

Fig. 3. Periodic model for the adsorption of oxygen molecule on the regular Al(001) slab (see explanation of graphic images in Fig. 2) with three possible adsorption sites: two horizontal positions over bridge and four-fold hollow sites and one vertical position above the same *fcc* site on the substrate. (a) Top view of the Al(001) substrate shows 2 × 2 surface supercell marked by a thicker line. (b) Three joined cross-sections of the same model as shown in (a) along the $Q_1-Q_1(110)$, $Q_2-Q_2(100)$ and $Q_3-Q_3(1\bar{1}0)$ planes. The small tetrahedra and octahedra show surface (o_B) and interstitial (t_{in} and o_A) sites of tetrahedral and octahedral symmetry, which are the preferred sites for the metastable location of oxygen ions.

for this interface performed recently by Yourdshahyan et al. [22] has confirmed that the 'molecularly chemisorbed' state of oxygen at *fcc* sites is characterized by an orientation of the molecular axis that is not parallel to the surface and by the transfer of 1.8 e from aluminum towards O_2.

Beginning with the almost spontaneous dissociation of $(O_2^-)_{ads}$ species up to the chemisorption of oxygen atoms (transition between (b) and (c) configurations in Table 4), the ground state is a singlet with energy differences of 0.2–0.4 eV along the dissociation trajectory and 0.9–1.1 eV for

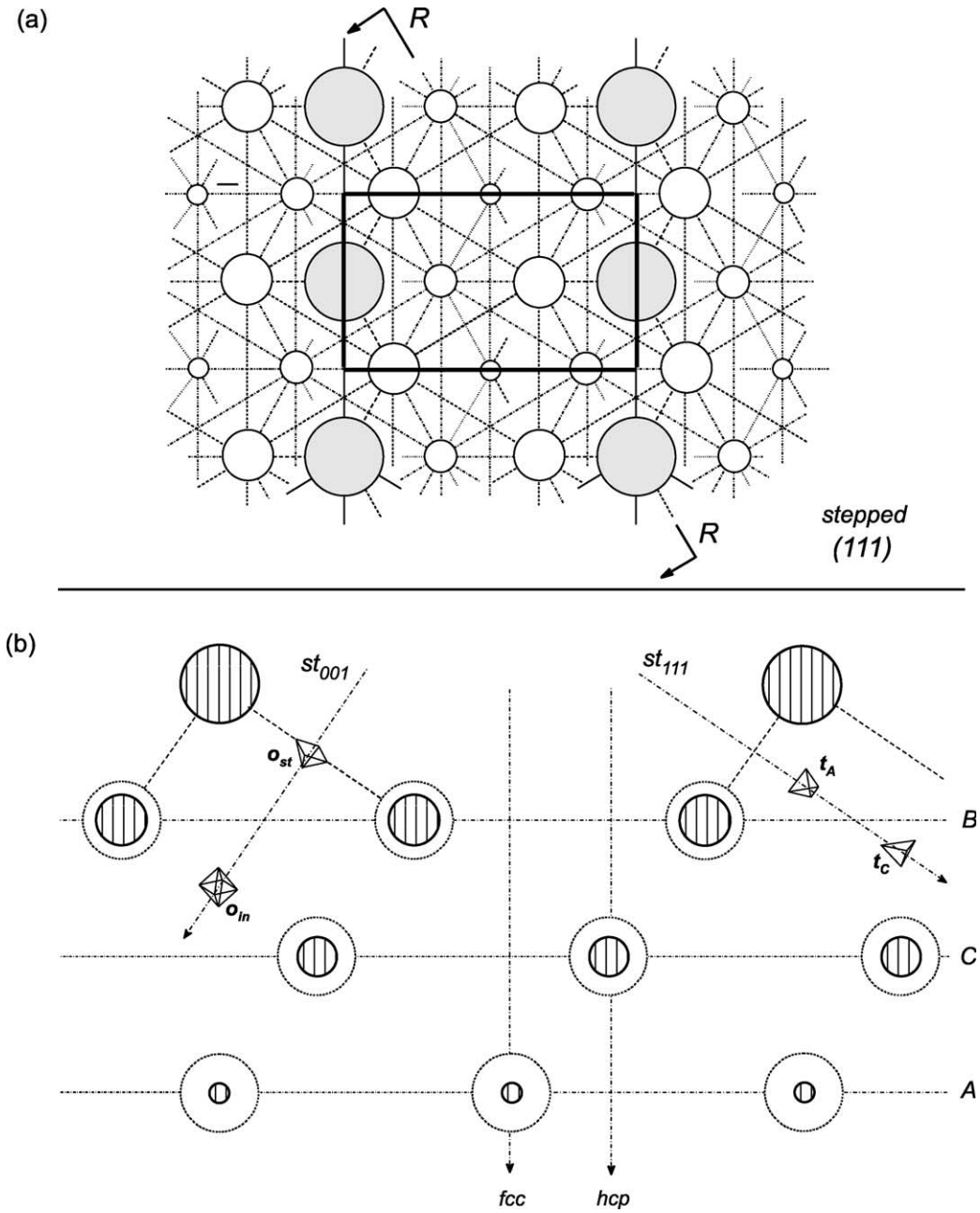

Fig. 4. Periodic model of the stepped O/Al(111) interface (see explanation of graphic images in Fig. 2) with possible positions of oxygen ions on regular steps containing both {111} and {001} microfacets as well as on pits of the aluminum substrate. (a) Top view of the stepped substrate shows that it differs from that for a perfect Al(111) surface (Fig. 2) by both the absence of every second row of outer Al atoms and the rectangular surface unit cell (instead of a rhombic one) marked by thicker lines. (b) Dash–dot arrows on the cross-section view (R–R) marked by *hcp* and *fcc* (over flat pits) as well as st_{001} and st_{111} (over the corresponding microfacets of regular steps) show four energetically favorable sites for chemisorption. The small tetrahedra and octahedra show surface (o_{st}) and interstitial (t_A, t_C and o_{in}) sites, which are the most suitable for metastable location of oxygen ions.

O_{ads} atoms. Dissociated atoms are rather adsorbed over adjacent sites as shown in Fig. 2(a), in agreement with STM observations by Schmid et al. [32]. Their chemisorption is accompanied by the transfer of further charge to give $\sim$0.9 e per adatom, i.e. closely approximating O^-_{ads} ions (cf. dissociating O_2^{2-} molecular ions described in Refs. [20,22]). The net energy released per oxygen ion, after molecular adsorption and dissociation, is 4.2 eV (Table 4).

Table 3
Properties of close-packed aluminum surfaces calculated for slab models of different thickness by using B/PWGGA functional: absolute (relative) vertical relaxation of the first interlayer Δl_{1-2} (δl_{1-2}), surface energy E_{surf}, change of electronic charge on the surface atoms Δq_{Al}^{surf} and Mulliken population of the bonds between them p_{Al-Al}^{surf} compared with corresponding experimental and theoretical data

Slab models and sources of data	$\Delta l_{1-2}(\delta l_{1-2})$, Å (%)	$E_{surf,}$ eV (erg/cm^2)	Δq_{Al}^{surf} [a] (e)	δp_{Al-Al}^{surf} [a] (e)
Regular Al(111) surface				
3-Layer	0.012 (0.5%)	0.596 (1449)	0.050	0.131
5-Layer	−0.013 (−0.56%)	0.524 (1274)	0.042	0.131
7-Layer	−0.029 (−1.2%)	0.468 (1138)	0.041	0.129
Experiments	(0%[b], 1%[c])	(1143)[d]	–[e]	–[e]
Other simulations	(−1.8%[f], −3.3%[g])	(1199)[h]	–[e]	–[e]
Regular Al(001) surface				
3-Layer	−0.015 (−0.7%)	0.656 (1595)	0.084	0.168
5-Layer	−0.034 (−1.7%)	0.562 (1367)	0.079	0.167
7-Layer	−0.049 (−2.4%)	0.527 (1282)	0.080	0.165
Experiments	(−2%[i], 0%[c])	–[e]	–[e]	–[e]
Other simulations	(−2.7%[f], −4.9%[g])	(1347)[h]	–[e]	–[e]
Stepped Al(111) surface				
5-Layer	−0.12 (−5.1%)	0.755 (1835)	0.88[j]	0.207[j]

[a] A positive sign for both Δq_{Al}^{surf} and p_{Al-Al}^{surf} means an excess of electron density.
[b] Neve et al. [72].
[c] Adams et al. [73].
[d] Tyson and Miller [66].
[e] No data were found in the literature.
[f] Berch et al. [74].
[g] Ning et al. [75].
[h] Vitos et al. [76].
[i] Masud et al. [77].
[j] For edge atoms on the steps.

The equilibrium distance of O_{ads}^- from the substrate is $z_O \approx 0.75$ Å (Table 5), in agreement with an experimental value of 0.7 ± 0.1 Å [33] and recent DFT simulations (0.71–0.77 Å [23]).

The next stage of initial oxidation is the absorption of O_{ads}^- ions (see (d) configuration in Table 4). Our calculations support the view that absorption of O_{ads}^- occurs randomly rather than uniformly over the whole Al(111) surface and that the 'pre-oxidized state' of Bylander and Kleinman [17] means an intermediate state in which oxygen ions are partially but not completely absorbed. According to the explanation in Section 1, clearly steric hindrance prevents synchronous absorption of an oxygen monolayer. Penetration of a certain O_{ads}^- ion into the Al(111) substrate is accompanied by reconstruction of the latter, which involves the symmetrical 10–12% enlargement of the equilateral triangle of Al atoms below this ion (Fig. 2(a)) and expansion of the first substrate interlayer under this triangle by 0.25–0.45 Å (depending on O_{ads}^- localization at the three different types of tetrahedral and octahedral interstices shown in Fig. 2(b)). This results in a significant decrease of the activation energy for oxygen penetration (from 2.5 to 1.4 eV per ion) and a marked increase in the binding energy of absorbed oxygen inside the substrate (from 8.3 to 9.7 eV per ion).

All the data presented in Table 5 for (c) and (d) configurations of the O/Al(111) interface (Table 4) refer to the fully relaxed geometry. Slight differences between results for a monolayer and 1/4 monolayer of O_{ads}^- are due to interactions within the adsorbed layer affecting the binding to the substrate. Our calculated binding energy E_{bind} per chemisorbed oxygen ion on *fcc* sites of 10.8 eV agrees with that from earlier DFT calculations of 10.7 eV for similar slab models [16,17]. E_{bind} is decreased to 9.2–9.7 eV on absorption of oxygen ions in three different interstices (Table 5). These values are somewhat larger than the 5–7 eV found for O/Al_n cluster models [7,9] and the 8 ± 1 eV found experimentally for the interaction of an Al_n cluster with O_2 [67]. However, such differences are hardly surprising since a large fraction of the atoms in an Al_n cluster are surface atoms and there is no crystal substrate. Our values quoted above are for the chemisorption and absorption of atomic oxygen and are reduced to 6.4–6.6 eV per O_{ads}^- ion when adsorption and dissociation of molecular oxygen is allowed for. Lower values for the same energy in a similar model (4.3–5.0 eV) were obtained in calculations performed by both Jacobsen et al. [18] and Kiejna and Lundqvist [23] using a plane-wave DFT method that employed the GGA approximation.

Table 4
Energy required at each step of the proposed mechanism for the oxidation of an Al(111) surface by O_2. (A negative value corresponds to energy evolved)

Reaction step:	Net energy absorbed (eV per oxygen atom)	Graphic images of interfacial cross-sections
(a) Remote O_2 molecules over Al(111) surface	0	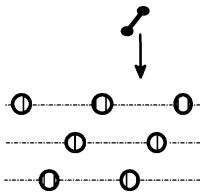
(b) Molecular adsorption	−2.6	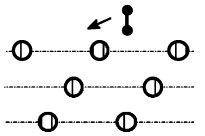
(c) Dissociation of $(O_2^-)_{ads}$ and chemisorption	−1.6	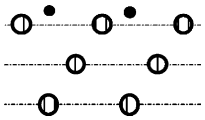
(d) Absorption of O_{ads}^- ions	1.4	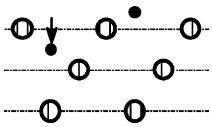
(e) Outward motion of external Al atoms	0.25	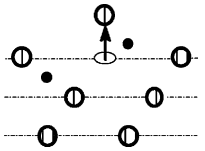
(f) Formation of the first Al_2O_3 formula units	0.2	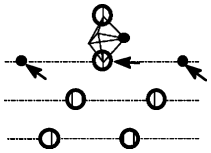
Net energy for the whole process $a \rightarrow f$	−2.3	

Fig. 5 shows two-dimensional (2D) difference electron charge density (ECHD) plots (that is, the ECHD in the relaxed configuration minus the sum of the ECHDs of the atoms before reaction) in a (110) plane that intersects the Al(111) surface along the line *PP* shown in Fig. 2(a). Corresponding changes in the energy gain per oxygen atom are given in Table 4. Fig. 5(a) shows an isolated O_2 molecule (with its axis parallel to the surface) lying above the surface along the line *PP*. Fig. 5(b) shows an adsorbed O_2^- molecular ion above the *fcc* hollow site. The extra charge density that makes *fcc* sites the preferred adsorption sites is clearly visible, as are areas of electron density around the upper oxygen atom which may be considered as 'dissociation channels'. Dissociation is highly favored energetically and Fig. 5(c) shows a monolayer of chemisorbed oxygen ions over *fcc* sites. The next step in the oxidation of Al is the absorption of O_{ads}^- in the first subsurface layer (Fig. 5(d)), which requires reconstruction of the Al(111) surface. Incorporation of O_{ads}^- into the substrate leads to both expansion of the subsurface interlayer and the transfer of further charge to oxygen ($\Delta q_O = 1.4 - 1.8$ e).

To describe the appearance of the first Al_2O_3 formula units in the O/Al(111) interface we propose a mechanism in which an Al atom moves outward from the surface, thus crossing a triangle formed from O_{ads}^- ions (see (e) configuration in Fig. 5 and Table 4), and then oxygen ions and aluminum atoms rearrange as in the configuration shown in (f). All the steps from the chemisorption of atomic oxygen to the formation of a molecular unit of Al_2O_3 require some energy (Table 4), though the sum total needed is much less than the 4.2 eV per oxygen ion available from adsorption and dissociation of an O_2 molecule. The net energy requirement for the whole process is −2.3 eV per O atom so that the mechanism proposed is quite feasible. With our current computing resources it was not possible to follow in detail the last step, which must involve further adsorption of oxygen (to satisfy stoichiometry) and aggregation of Al_2O_3 units to form a growth nucleus. Probably Al_2O_3 quasi-molecules can catalyze the formation of others on nearest-neighbor sites. Because of the very high cohesive energy of crystalline Al_2O_3 one can anticipate that the aggregation of Al_2O_3 units to form $(Al_2O_3)_n$ will soon become quite exothermic with increasing n.

In their latest paper Kiejna and Lundqvist [24] consider an optimized ultrathin oxide film on the Al(111) substrate and the interface between them (regular slab model) but no attempts have been made to simulate the intermediate stage of Al_2O_3 aggregation. Comprehensive Monte-Carlo simulations of the initial Al(111) oxidation performed recently by Chakarova et al. [28] could consider a $400 \times 400 \times 6$ cluster model with different temperatures and oxygen coverages. But Monte-Carlo simulations cannot take into account changes in electronic structure, including the strong chemical interaction due to the high affinity of oxygen for aluminum. Nor can they describe the mechanism of the initial oxidation at the level of elementary Al_2O_3 formula units. An STM study by Brune et al. [31] of carefully prepared samples of the Al(111) substrate before its interaction with oxygen showed the presence of terraces, steps and kinks. It is known from various studies of chemisorption that surface defects not only strengthen bonding between a metallic substrate and an adsorbate but also initiate surface reactions [4]. This is why we have

Table 5
Properties of regular O/Al(111) interface (Fig. 2) for various locations of chemisorbed and absorbed oxygen ions as well as for two different substrate coverages

Oxygen ion over or in:	Type of configuration in interface	Distance z_O[a] (Å)	Induced charge Δq_O[b] (e)	Binding energy E_{bind}(O/Al) (eV)
Oxygen monolayer				
o_C center	Chemisorption	0.74	0.92	10.82
	Absorption	−1.45	1.69	9.36
t_B center	Chemisorption	0.76	0.84	10.57
	Absorption	−0.75	1.07	9.21
t_A center	Absorption	−1.77	1.39	9.66
1/4 Oxygen monolayer				
o_C center	Chemisorption	0.77	0.95	10.45
	Absorption	−1.38	1.75	9.39
t_B center	Chemisorption	0.79	0.86	10.22
	Absorption	−0.72	1.32	9.16
t_A center	Absorption	−1.77	1.45	9.62

[a] z_O is determined regarding external layer of the substrate.
[b] For an explanation of the sign of Δq_O see Table 3.

begun DFT simulations on a slab model of the stepped O/Al(111) interface, as described briefly in Section 6.

5. Interaction of oxygen with a regular Al(001) substrate

To simulate the molecular O_2 adsorption we used mainly a 2 × 2 SC (Fig. 3) which corresponds to $\theta_O = 0.5$ coverage of substrate by chemisorbed adatoms after dissociation. For atomic chemisorption we considered both a monolayer of atomic oxygen (1 × 1 UC), i.e. $\theta_O = 1$, and a 1/4 atomic oxygen adlayer on the Al(001) substrate ($\theta_O = 0.25$). Both coverages were also considered in order to study the penetration of oxygen adatoms into the substrate.

The oxygen interaction with (001) substrate begins with the same initial geometry of a free O_2 molecule as described in Section 4 for the regular Al(111) surface. Unlike the latter case, the horizontal position of $(O_2)_{ads}$ above the four-fold *fcc* site on Al(001) surface (o_B *center*) is preferred (as shown in Fig. 3). This difference is the cause of symmetry–compatibility of a linear O_2 molecule with an (001)

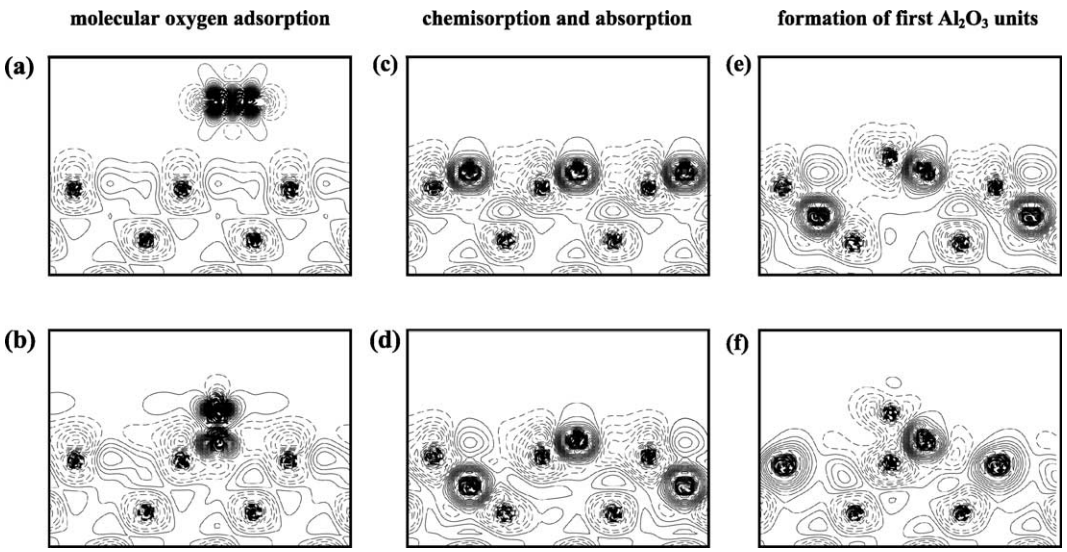

Fig. 5. Difference electron density plots describing the charge distribution in the (a) to (f) configurations of regular O/Al(111) interface shown in Table 4, relative to that of free Al and O atoms. Accumulation of electronic charge is shown by solid lines, while dashed lines show a deficit of charge with respect to the free atoms. Isodensity curves are drawn from −1 to +1 e au^{-3} with increments of 0.002 e au^{-3} (1 au = 1 Bohr).

substrate, in contrast to the (111) surface. The triplet state of an adsorbed oxygen molecule above the (001) surface is also more stable than the singlet state, by 1.0–1.1 eV, which is even larger than above the (111) surface. Also, molecular adsorption on Al(001) is accompanied by a larger charge transfer from external aluminum atoms (1.15 e per molecule versus 0.9 e, as indicated in Section 4). Saddle points in surface energy are practically absent along the trajectories of spontaneous dissociation of molecular oxygen above the Al(001) substrate (Fig. 3(a)), even above the bridge (*br*) sites. This is probably due to the higher position of $(O_2^-)_{ads}$ above the (001) surface (1.26 Å versus 1.16 Å for the distance to the lower intramolecular atom in a (111) surface). The change of ground state during $(O_2^-)_{ads}$ dissociation from triplet to singlet is quantitatively similar for both (001) and (111) surfaces. Localization of adatoms above neighboring o_B centers is accompanied by the transfer of further charge to give 1.0–1.2 e, somewhat larger than above an Al(111) surface. This is also true for the total value of net energy after molecular adsorption and dissociation, 4.3 eV versus 4.2 eV (Section 4). These data may be considered as additional confirmation of conclusions made in earlier studies about the greater reactivity of the Al(001) surface towards oxidation [1], even during the initial stage of molecular adsorption.

The main results of our simulations on the regular O/Al(001) interface are presented in Table 6 for the particular relaxed geometry studied. (We simulate vertical relaxation only, not horizontal reconstruction as in the case of the regular O/Al(111) interface). Both equilibrium values of z_O over *fcc* hollow sites have been found to be ~0.5 Å, closer to the surface than for the O/Al(111) interface. We also consider oxygen chemisorption above bridge sites on the Al(001) substrate in which the adsorbate is positioned above tetrahedral t_{in} centers of the subsurface lattice (Fig. 3) because some experiments gave indirect confirmation of the existence of these interface configurations [1,36]. The equilibrium position of oxygen above bridge sites is higher (~0.85 Å), due to the smaller coordination of surface Al atoms. A smaller induced charge Δq_O is concentrated on an adatom localized above a *br* site since this is not a proper position for chemisorption but a saddle point for the surface diffusion of O_{ads}^- ions. The binding energy E_{bind} per oxygen ion above the four-fold *fcc* site is practically the same as above the *fcc* site on the Al(111) surface (10.5–10.9 eV). Though the value of z_O for the O/Al(001) interface is smaller, lateral interactions are also smaller than for the Al(111) substrate: in the case of monolayer coverage of the Al(001) surface each O atom has four nearest oxygen neighbors instead of six. For oxygen ions localized above the *br* sites, E_{bind} is considerably smaller (9.6 eV). Outward relaxation of the external substrate layer in the case of monolayer oxygen chemisorption on Al(001) is larger than for the *fcc* of the O/Al(111) interface, being 0.2 Å instead of 0.07 Å. For a *br* site, it is noticeably smaller (0.08 Å), since this value must depend upon the distance between adsorbate and adsorbent.

As mentioned above, unlike the Al(111) surface, the less dense Al(001) plane does not hinder the penetration of oxygen ions into the substrate through its *fcc* hollow sites o_B (Fig. 3). The energy barriers for oxygen penetration into subsurface interstices via *fcc* hollow sites are different as well for Al(001) and Al(111) substrates (0.8 eV versus 1.4 eV for one quarter oxygen coverage), Moreover, unlike the O/Al(111) interface, the binding energy of an oxygen ion localized at the t_{in} center is higher by 0.3 eV than that for O_{ads}^- chemisorbed above the four-fold site on the Al(001) surface. (This is for the model of monolayer coverage; in the case of 1/4 coverage chemisorption and absorption energies are almost equal). However, this effect may be observed in our simulations only after the marked outward relaxation of the external substrate layer (by ~0.6 Å), when oxygen ions

Table 6
Properties of regular O/Al(001) interface (Fig. 3) for various locations of chemisorbed and absorbed oxygen ions as well as for two different substrate coverages

Oxygen ion over or in:	Type of configuration in interface	Distance z_O [a] (Å)	Induced charge Δq_O [b] (e)	Binding energy E_{bind}(O/Al) (eV)
Oxygen monolayer				
o_B center	Chemisorption	0.51	1.23	10.84
t_{in} center	Chemisorption	0.85	0.64	9.63
	Absorption	−1.32	1.42	11.12
o_A center	Absorption	−2.44	1.64	10.07
1/4 Oxygen monolayer				
o_B center	Chemisorption	0.53	1.01	10.43
t_{in} center	Chemisorption	0.88	0.59	9.47
	Absorption	−1.25	1.35	10.42
o_A center	Absorption	−2.30	1.73	9.91

[a] For an explanation of z_O see Table 5.
[b] For an explanation of the sign of Δq_O see Table 3.

move towards t_{in} centers. These calculations confirm results obtained earlier by Bedford and Kunz [8] for the cluster model of the O/Al(001) interface and show that the most stable position for absorbed oxygen ions is at the t_{in} center. At the same time, incorporation of O^-_{ads} via bridge sites is doubtful, even with structural reconstruction of the Al(001) substrate. Localization of oxygen ions at t_{in} centers could possibly be due to internal diffusion ($o_B \rightarrow t_{in}$). As in the case of the O/Al(111) interface, penetration of O^-_{ads} into the (001) substrate leads to both expansion of the subsurface interlayer and the transfer of further charge to oxygen ($\Delta q_O = 1.4 - 1.75$ e). The similarity of the induced charges in both substrates may be explained by the similar coordination of absorbed oxygen ions. On the whole, comparison of data presented in Tables 5 and 6 is a good argument in favor of faster oxidation of the Al(001) surface compared to Al(111) as observed experimentally [1,36]. This also explains why the chemisorption stage of oxidation on Al(001) substrate is less marked than on Al(111).

6. Interaction of oxygen with a stepped Al(111) substrate

Recent theoretical simulations of homoepitaxial growth of the Al(111) substrate performed by Bogicevic et al. [42] and confirmed by the corresponding STM study by Barth et al. [43], establish two main types of steps: the A-step with a {001} microfacet and the B-step with a {111} microfacet. In our model (Fig. 4), the {001} and {111} microfacets correspond precisely with the A- and B-steps of epitaxially grown islands on the Al(111) surface, respectively. Therefore, this stepped model reproduces accurately fragments of the real Al(111) substrate.

Results of calculations on the stepped O/Al(111) interface with coverage $\theta_O = 0.25$ are presented in Table 7 for a particular relaxed geometry (we simulate vertical relaxation only, not horizontal reconstruction as in the case of regular O/Al(111) interface). Due to computational limitations we could not optimize the equilibrium configuration of oxygen in different chemisorption and absorption positions as carefully as was done for the regular O/Al(111) and O/Al(001) interfaces. Therefore, these results should be interpreted more as a starting point for further more comprehensive studies than as results of the quality of those reported for the regular Al(111) and Al(001) substrates. Nevertheless, two distinctive peculiarities of the model for a stepped O/Al(111) interface can be mentioned here:

- the presence of {001} microfacets on the surface steps makes penetration of oxygen ions into the substrate much easier than in the case of regular O/Al(111) interface, although calculated parameters of oxygen ions absorbed by the stepped substrate (Table 7) are close to those described above for O^-_{ads} localized in interstitial sites of regular Al(111) substrate (with the same 1/4 oxygen coverage, Table 5);
- simulation of oxide nucleation on the stepped surface should show it to be more effective than the corresponding model of the perfect interface which is described in Section 4, but would require more extensive computational resources due to its lower symmetry.

We have simulated all four positions for oxygen chemisorption shown in Fig. 4 (st_{001}, st_{111}, *fcc* and *hcp*) although bonding of O^-_{ads} ions over triangle st_{111} sites (with two Al atoms positioned on the edge of step) is much weaker than in the other three positions. (This is why we did not include the corresponding data in Table 7.) Due to the stepped structure of substrate with the marked influence of its edges on chemisorption the equilibrium distances from adatoms down to the corresponding sites on flat pits and microfacets of steps (Table 7) are larger than for the perfect O/Al(111) and O/Al(001) interfaces (cf. Tables 5 and 6 for the same 1/4 oxygen coverage). Adatoms above both st_{001} and st_{111} sites are somewhat higher than the edges of steps (on 0.4 and 0.6 Å, respectively), but above *fcc* and *hcp* sites they are

Table 7
Properties of stepped O/Al(111) interface (Fig. 4) for various locations of chemisorbed and absorbed oxygen ions

Oxygen ion over or in:	Type of configuration in interface	Distance z_O[a] (Å)	Induced charge Δq_O[b] (e)	Binding energy E_{bind}(O/Al),
o_{st} center	Chemisorption	1.85	0.83	11.31
t_A center	Absorption	−1.85	1.35	10.68
t_C center	Absorption	−0.71	1.39	9.93
o_{in} center	Absorption	−1.31	1.81	10.11
fcc 'pit' site	Chemisorption	0.87	1.07	10.83
hcp 'pit' site	Chemisorption	1.11	0.96	10.61

[a] For chemisorption of oxygen ion above o_{st} center, z_O means a vertical z-projection of the distance between O^-_{ads} and this position; for absorption of oxygen at t_A center, z_O is a vertical distance between the latter position and edge of the step; in other chemisorption and absorption positions of O^-_{ads}, z_O is determined regarding a second (pit) layer of the substrate.
[b] For an explanation of the sign of Δq_O see Table 3.

localized inside substrate pits. The proximity of the corresponding edge to the nearest adatom is also important (Table 7): an O^-_{ads} ion is most affected when in the st_{001} or st_{111} position. The chemisorption trajectories are rather curved in both cases, compared to the straight lines in Fig. 4. An *fcc* position for oxygen, being further away from the edge of step, is influenced to a smaller extent and calculated parameters in this case are close to those for the perfect O/Al(111) interface (Table 5).

It is quite reasonable that the most energetically preferred position of O^-_{ads} on the stepped Al(111) surface is found to be st_{001} site. The binding energy for oxygen chemisorption in this case is somewhat higher than over both perfect Al(111) and Al(001) surfaces in the same case of 1/4 coverage ($\sim$11.3 eV). The most preferred absorption center t_A inside the substrate step (Fig. 4) is the one closest to this st_{001} site. Localization of an oxygen ion in this tetrahedral center leads to an outward relaxation of the edge of the step of up to 0.6 Å. The ratio of energies between absorbed and chemisorbed states at the stepped O/Al(111) interface show that oxygen penetration into the substrate along the $st_{001} \rightarrow t_A$ direction is more favorable than for the regular O/Al(111) interface but less favorable than for the O/Al(001) interface: the difference of their energies for 1/4 coverage being $-0.8\ \text{eV} < -0.6\ \text{eV} < 0\ \text{eV}$. Thus, the presence of the {001} microfacets on the stepped Al(111) surface leads to easier absorption of O^-_{ads} ions. The energy barrier of oxygen penetration is $\sim$1.1 eV through the surface site o_{st} (Fig. 4) and is thus comparable with the energy barriers (0.8–1.4 eV) given in Sections 4 and 5 for regular interfaces. This activation barrier for oxygen absorption could be even lower if we could have simulated surface reconstruction as was done for the perfect O/Al(111) interface with 1/4 oxygen coverage.

Charge analysis (Table 7) indicates rather underestimated values of Δq_O in chemisorption and absorption positions of oxygen in the vicinity of each step (st_{001}, st_{111} and t_A) as compared to both perfect interfaces (Tables 5 and 6 for 1/4 substrate coverage) although the deeper chemisorption and absorption positions of O (*fcc*, *hcp*, o_{in} and t_C) the values of Δq_O are higher. Probably this is due to either reduced or enhanced electron density around the step or pit (Fig. 4), as was recently shown by us in 2D ECHD of the stepped Al(111) substrate [60]. Its vertical relaxation leads to increase of both E_{bind} and Δq_O. Probably the most realistic model for the O/Al(111) interface would be 'islands' on this substrate, as considered in Ref. [42], but such a model is too complicated for periodic first principles simulations.

7. Conclusions

- As shown by our calculated values of the aluminum lattice constant, bulk modulus, conduction-band width and electronic energies at high symmetry points the DFT CO LCGTF method is a reliable computational tool, particularly when used with B/PWGGA functionals [47,48].
- Calculations of electrostatic potentials across the close-packed slabs of Al [60] show that the surface perturbation is confined mainly to the outer layer. Calculated values of the surface energy for 5- and 7-layer slabs are in satisfactory agreement with experiment and this indicates that reliable conclusions concerning energies may be drawn from slabs, even when these contain only 5 or 7 layers.
- Contact with oxygen molecules leads to their adsorption in the triplet electronic ground state. The most favorable configuration of the adsorbed O_2 molecules on Al(111) is perpendicular to the surface above three-fold *fcc* sites whereas on Al(001) substrate the preferable position of molecular adsorption is parallel to the surface above four-fold *fcc* sites. In both cases adsorption is accompanied by ionization to form $(O^-_2)_{ads}$. Dissociation occurs almost spontaneously, with negligible energy barrier in the case of (111) substrate and its complete absence for (001) substrate, in order to form singlet chemisorbed O^-_{ads} ions accompanied by the release of energy amounting to 4.2–4.3 eV per ion.
- The chemisorbed oxygen ions occupy three-fold *fcc* and/or *hcp* sites on regular Al(111) substrate at distances of 0.74 and 0.76 Å from the surface, with binding energies of 10.8 and 10.6 eV per ion, respectively. On regular Al(001) surface, O^-_{ads} ions prefer four-fold *fcc* sites with localization at $z_O \approx 0.5$ Å, with binding energies of 10.8 eV per ion. The energetically most favorable position for chemisorption of O^-_{ads} ions was found to be over stepped Al(111) surface, above o_{st} center (0.4 Å over the edge of step): $E_{bind} = 11.3$ eV per ion.
- Chemisorbed O^-_{ads} can penetrate into the regular (111), stepped (111) and regular (001) substrates with activation energies of 1.4, 1.1 and 0.8 eV, respectively. For the (111) substrate, this process cannot occur uniformly over a monolayer of O^-_{ads} since it requires longitudinal surface-layer reconstruction, involving an 11% expansion of Al equilateral triangles to allow the passage of oxygen ions into the subsurface layer. The less dense Al(001) plane does not hinder oxygen ions penetration into the substrate through its four-fold *fcc* sites at all, the same is true for absorption of O^-_{ads} ions through {001} microfacets on the stepped Al(111) substrate. Absorption is accompanied by further ionization so that the absorbed O^-_{ads} ions have a charge of -1.4 to -1.8 e (depending on their location inside the substrate).
- In this paper we have proposed an energetically feasible mechanism of the reaction of O_2 with regular Al(111) up to the formation of Al_2O_3 quasi-molecules. A periodic net of isolated Al_2O_3 formula units would be unstable with respect to chemisorbed O^-_{ads} ions so that aggregation of Al_2O_3 units evidently occurs rapidly. Probably each Al_2O_3 unit formed catalyzes the formation of adjacent ones until a stable growth nucleus is formed, but this last

step could not be simulated with current computer resources. A cluster model might be tried, but this would have the disadvantage that there is no crystalline Al substrate. The influence of substrate defects on the mechanism of Al(111) oxidation should be considered.

Acknowledgements

This study was supported by the Natural Sciences and Engineering Research Council of Canada and the European Centre of Excellence for Advanced Materials Research and Technology under Contract ICA1-CT-2000-7007. Yu.Z. and M.C. thank the Centre for Chemical Physics at the University of Western Ontario for financial support under its Fellowship and Visitor programs. The authors thank E. Heifets, A. Kokalj, B.I. Lundqvist, Yu.N. Shunin, and A.M. Stoneham for helpful discussions. The technical assistance of Yu. Mastrikov and O. Sychev was most valuable.

References

[1] I.P. Batra, L. Kleinman, J. Electron Spectrosc. Relat. Phenom. 33 (1984) 175.
[2] N. Cabrera, N.F. Mott, Rep. Progr. Phys. 12 (1948) 163.
[3] F.P. Fehlner, N.F. Mott, Oxid. Metals 2 (1970) 59.
[4] M.W. Roberts, C.S. McKee, Chemistry of the Metal–Gas Interface, Clarendon Press, Oxford, 1978.
[5] R.P. Messmer, D.R. Salahub, Phys. Rev. B 16 (1977) 3415.
[6] D.R. Salahub, M.R. Roche, R.P. Messmer, Phys. Rev. B 18 (1978) 6495.
[7] B.N. Cox, C.W. Bauschlicher, Surf. Sci. 115 (1982) 15.
[8] K.L. Bedford, A.B. Kunz, Phys. Rev. B 25 (1982) 2119.
[9] G. Pacchioni, P. Fantucci, Surf. Sci. 204 (1988) 587.
[10] P.S. Bagus, C.R. Brundle, F. Illas, F. Parmigiani, G. Polzonetti, Phys. Rev. B 44 (1991) 9025.
[11] N.D. Lang, A.R. Williams, Phys. Rev. Lett. 34 (1975) 531.
[12] I.P. Batra, S. Ciraci, Phys. Rev. Lett. 39 (1977) 774.
[13] D.S. Wang, A.J. Freeman, H. Krakauer, Phys. Rev. B 24 (1981) 3092 & 3104.
[14] H. Krakauer, M. Posternack, A.J. Freeman, D.D. Koelling, Phys. Rev. B 23 (1981) 3859.
[15] I.P. Batra, O. Bisi, Surf. Sci. 123 (1982) 283.
[16] D.M. Bylander, L. Kleinman, K. Mednick, Phys. Rev. Lett. 48 (1982) 1544.
[17] D.M. Bylander, L. Kleinman, Phys. Rev. B 28 (1983) 1090.
[18] J. Jacobsen, B. Hammer, K.W. Jacobsen, J.K. Nørskov, Phys. Rev. B 52 (1995) 14954.
[19] T. Sasaki, T. Ohno, Phys. Rev. B 60 (1999) 7824.
[20] K. Honkala, K. Laasonen, Phys. Rev. Lett. 84 (2000) 705.
[21] Yu.F. Zhukovskii, O. Sychev, P.W.M. Jacobs, Yu.N. Shunin, Comput. Model. New Technol. 4 (2) (2000) 18.
[22] Y. Yourdshahyan, B. Razaznejad, B.I. Lundqvist, Solid State Commun. 117 (2001) 531. Y. Yourdshahyan, B. Razaznejad, B.I. Lundqvist, Phys. Rev. B. 65 (2002) 075416.
[23] A. Kiejna, B.I. Lundqvist, Phys. Rev. B 63 (2001) 085405. A. Kiejna, B.I. Lundqvist, Phys. Rev. B 64 (E) (2001) 049901.
[24] A. Kiejna, B.I. Lundqvist, Surf. Sci. 504 (2002) 1.
[25] C. Engdahl, G. Wahnström, Surf. Sci. 312 (1994) 429.
[26] G. Wahnström, A.B. Lee, J. Strömquist, J. Chem. Phys. 105 (1996) 326.
[27] R.L. Strong, B. Firey, F.W. De Wette, J.L. Erskine, Phys. Rev. B 26 (1982) 3483.
[28] R. Chakarova, D.E. Oner, I. Zoric, B. Kasemo, Surf. Sci. 472 (2001) 63.
[29] J. Stöhr, L.I. Johansson, S. Brennan, M. Hecht, J.N. Müller, Phys. Rev. B 22 (1980) 4052.
[30] L.L. Lauderback, A.J. Lynn, C.J. Waltman, S.A. Larson, Surf. Sci. 243 (1991) 323.
[31] H. Brune, J. Wintterlin, J. Trost, G. Ertl, J. Wiechers, R.J. Behm, J. Chem. Phys. 99 (1993) 2128.
[32] M. Schmid, G. Leonardelli, R. Tscheließnig, A. Biedermann, P. Varga, Surf. Sci. 478 (2001) L355.
[33] M. Kerkar, D. Fischer, D.P. Woodruff, B. Cowie, Surf. Sci. 271 (1992) 45.
[34] S.A. Flodström, C.W. Martinsson, R.Z. Bachrach, S.B.M. Hangström, R.S. Bauer, Phys. Rev. Lett. 40 (1978) 907.
[35] C. Berg, S. Raaen, A. Borg, J.N. Andersen, E. Lundgren, R. Nyholm, Phys. Rev. B 47 (1993) 13063.
[36] R. Michel, J. Gastaldi, C. Allasia, C. Jourdan, J. Derrien, Surf. Sci. 95 (1980) 309.
[37] R.Z. Bachrach, G.V. Hansson, R.S. Bauer, Surf. Sci. 109 (1981) L560.
[38] J. Hitzke, J. Günster, J. Kolaczkiewicz, V. Kempter, Surf. Sci. 318 (1994) 139.
[39] L.P.H. Jeurgens, W.G. Sloof, C.G. Borsboom, F.D. Tichelaar, E.J. Mittemeijer, Appl. Surf. Sci. 161 (2000) 139.
[40] J.E. Crowell, J.G. Chen, J.T. Yates, Surf. Sci. 165 (1986) 37.
[41] V.E. Zhukov, I. Popova, J.T. Yates, Surf. Sci. 441 (1999) 251.
[42] A. Bogicevic, J. Strömquist, B.I. Lundqvist, Phys. Rev. Lett. 81 (1998) 637.
[43] J.V. Barth, H. Brune, B. Fischer, J. Weckesser, K. Kern, Phys. Rev. Lett. 84 (2000) 1732.
[44] V.R. Saunders, R. Dovesi, C. Roetti, M. Causá, N.M. Harrison, C.M. Zicovich-Wilson, CRYSTAL'98. User Manual, Turin University, 1999.
[45] P.A.M. Dirac, Proc. Cambridge Phil. Soc. 26 (1930) 736.
[46] S.H. Vosko, L. Wilk, M. Nusair, Can. J. Phys. 58 (1980) 1200.
[47] A.D. Becke, Phys. Rev. A 38 (1988) 3098.
[48] J.P. Perdew, Y. Wang, Phys. Rev. B 45 (1992) 13244.
[49] A. Kokalj, A. Lesar, M. Hodoscek, M. Causá, J. Phys. Chem. B 103 (1999) 7222.
[50] K. Doll, N.M. Harrison, Chem. Phys. Lett. 317 (2000) 282.
[51] M.F. Guest, V.R. Saunders, Mol. Phys. 28 (1974) 819.
[52] V.L. Moruzzi, J.F. Janak, A.R. Williams, Calculated Electronic Properties of Metals, Pergamon Press, New York, 1978.
[53] H.J. Monkhorst, J.D. Pack, Phys. Rev. B 13 (1976) 5188.
[54] G. Gilat, J. Comput. Phys. 10 (1972) 390.
[55] M.D. Towler, A. Zupan, M. Causá, Comput. Phys. Commun. 98 (1996) 181.
[56] J.C. Boettger, U. Birkenheuer, N. Rösch, S.B. Trickey, Int. J. Quant. Chem. 28 (1994) 675.
[57] M. Causá, R. Dovesi, C. Pisani, C. Roetti, Phys. Rev. B 33 (1986) 1308.
[58] E. Heifets, E.A. Kotomin, R.I. Eglitis, J. Maier, G. Borstel, Phys. Rev. B 64 (2001) 235417.

[59] W.H. Press, S.A. Teukolsky, W.T. Vetterling, B.P. Flannery, Numerical Recipes in FORTRAN77, second ed., University Press, Cambridge, MA, 1997.
[60] P.W.M. Jacobs, Yu.F. Zhukovskii, Yu. Mastrikov, Yu.N. Shunin, Comput. Model. New Technol. 6 (1) (2002) 7.
[61] I. Baraille, C. Pouchan, M. Causá, F. Marinelli, J. Phys.: Condens. Matter 10 (1998) 10969.
[62] A. Kokalj, M. Causá, J. Phys.: Condens. Matter 11 (1999) 7463.
[63] S.P. Singhal, J. Callaway, Phys. Rev. B 16 (1977) 1744.
[64] F. Szmulowicz, B. Segall, Phys. Rev. B 24 (1981) 892.
[65] J.E. Inglesfield, Progr. Surf. Sci. 20 (1985) 105.
[66] W.R. Tyson, W.A. Miller, Surf. Sci. 62 (1977) 267.
[67] M.F. Jarrold, J.E. Brower, J. Chem. Phys. 87 (1987) 1610 & 5728.
[68] M.E. Straumanis, C.L. Woodard, Acta Cryst. A 27 (1971) 549.
[69] J.L. Tallon, A. Wolfenden, J. Phys. Chem. Solids 40 (1979) 831.
[70] A.P. Sutton, J. Chen, Phil. Mag. Lett. 61 (1990) 139.
[71] H.J. Levinson, F. Greuter, E.W. Plummer, Phys. Rev. B 27 (1983) 727.
[72] J. Neve, J. Rundgren, P. Westria, J. Phys. C 15 (1982) 4391.
[73] D.L. Adams, V. Jensen, X.F. Sun, J.H. Vollesen, Phys. Rev. B 38 (1988) 7913.
[74] A.V. Berch, S.V. Eremeev, A.G. Lipnitskii, I.Yu. Sklyadneva, E.V. Chulkov, Phys. Solid State 36 (1994) 1562.
[75] T. Ning, Q. Yu, Y. Ye, Surf. Sci. 206 (1988) L857.
[76] L. Vitos, A.V. Ruban, H.L. Skriver, J. Kollar, Surf. Sci. 411 (1998) 186.
[77] N. Masud, R. Bandoing, D. Aberdam, C. Gaubert, Surf. Sci. 133 (1983) 580.